

CALIS - a CALibration Insertion System for the DarkSide-50 dark matter search experiment

P. Agnes^a, T. Alexander^{ae}, A. Alton^b, K. Arisaka^{ad}, H.O. Back^x,
B. Balding^g, K. Biery^g, G. Bonfini^q, M. Bossaⁱ, A. Brigatti^s, J. Brodsky^x,
F. Budano^y, L. Cadonati^{ae}, F. Calaprice^x, N. Canci^{ad}, A. Candela^q,
H. Cao^x, M. Cariello^h, P. Cavalcante^q, A. Chavarria^d, A. Chepurnov^t,
A.G. Cocco^u, L. Crippa^s, D. D'Angelo^s, M. D'Incecco^q, S. Davini^k,
M. De Deo^q, A. Derbin^v, A. Devoto^c, F. Di Eusonio^x, G. Di Pietro^s,
E. Edkins^j, A. Empl^k, A. Fan^{ad}, G. Fiorillo^u, K. Fomenko^f, G. Forster^{ae},
D. Franco^a, F. Gabriele^q, C. Galbiati^x, A. Goretti^x, L. Grandi^d,
M. Gromov^t, M.Y. Guan^l, Y. Guardincerri^g, B. Hackett^j, K. Herner^g,
E.V. Hungerford^k, Al. Ianni^q, An. Ianni^x, C. Jollet^{aa}, K. Keeter^e,
C. Kendziora^g, S. Kidner^{af,1}, V. Kobylevⁿ, G. Koh^x, D. Korablev^f,
G. Korga^k, A. Kurlej^{ae}, P.X. Li^l, B. Loer^x, P. Lombardi^s, C. Love^{ab},
L. Ludhova^s, S. Luitz^z, Y.Q. Ma^l, I. Machulin^{o,r}, A. Mandaranoⁱ, S. Mari^y,
J. Maricic^j, L. Marini^y, C.J. Martoff^{ab}, A. Meregaglia^{aa}, E. Meroni^s,
P.D. Meyers^{x,*}, R. Milincic^j, D. Montanari^g, A. Monte^{ae}, M. Montuschi^q,
M.E. Monzani^z, P. Mosteiro^x, B. Mount^e, V. Muratova^v, P. Musico^h,
A. Nelson^x, S. Odrowski^q, M. Okounkova^x, M. Orsini^q, F. Ortica^w,
L. Pagani^h, M. Pallavicini^h, E. Pantic^{ad,ac}, L. Papp^{af}, S. Parmeggiano^s,
R. Parsells^x, K. Pelczar^m, N. Pelliccia^w, S. Perasso^a, A. Pocar^{ae},
S. Pordes^g, D. Pugachev^o, H. Qian^x, K. Randle^{ae}, G. Ranucci^s,
A. Razeto^q, B. Reinhold^j, A. Renshaw^{ad}, A. Romani^w, B. Rossi^{x,u},
N. Rossi^q, S.D. Rountree^{af}, D. Sablone^k, P. Saggese^q, R. Saldanha^d,
W. Sands^x, S. Sangiorgio^p, E. Segreto^q, D. Semenov^v, E. Shields^x,
M. Skorokhvatov^{o,r}, O. Smirnov^f, A. Sotnikov^f, C. Stanford^x,
Y. Suvorov^{ad}, R. Tartaglia^q, J. Tatarowicz^{ab}, G. Testera^h, A. Tonazzo^a,
E. Unzhakov^v, R.B. Vogelaar^{af}, M. Wada^x, S. Walker^u, H. Wang^{ad},
Y. Wang^l, A. Watson^{ab}, S. Westerdale^x, M. Wojcik^m, A. Wright^x,
X. Xiang^x, J. Xu^x, C.G. Yang^l, J. Yoo^g, S. Zavatarelli^h, A. Zec^{ae}, C. Zhu^x,
G. Zuzel^{lm}

*Corresponding authors.

Email address: meyers@princeton.edu (P.D. Meyers)

¹Deceased

- ^aAPC, Université Paris Diderot, Sorbonne Paris Cité, Paris 75205, France
^bPhysics and Astronomy Department, Augustana College, Sioux Falls, SD 57197, USA
^cPhysics Department, Università degli Studi and INFN, Cagliari 09042, Italy
^dKavli Institute, Enrico Fermi Institute and Dept. of Physics, University of Chicago, Chicago, IL 60637, USA
^eSchool of Natural Sciences, Black Hills State University, Spearfish, SD 57799, USA
^fJoint Institute for Nuclear Research, Dubna 141980, Russia
^gFermi National Accelerator Laboratory, Batavia, IL 60510, USA
^hPhysics Department, Università degli Studi and INFN, Genova 16146, Italy
ⁱGran Sasso Science Institute, L'Aquila 67100, Italy
^jDepartment of Physics and Astronomy, University of Hawai'i, Honolulu, HI 96822, USA
^kDepartment of Physics, University of Houston, Houston, TX 77204, USA
^lInstitute of High Energy Physics, Beijing 100049, China
^mSmoluchowski Institute of Physics, Jagiellonian University, Krakow 30059, Poland
ⁿInstitute for Nuclear Research, National Academy of Sciences of Ukraine, Kiev 03680, Ukraine
^oNational Research Centre Kurchatov Institute, Moscow 123182, Russia
^pLawrence Livermore National Laboratory, 7000 East Avenue, Livermore, CA 94550
^qLaboratori Nazionali del Gran Sasso, Assergi (AQ) 67010, Italy
^rNational Research Nuclear University MEPhI (Moscow Engineering Physics Institute), 115409 Moscow, Russia
^sPhysics Department, Università degli Studi and INFN, Milano 20133, Italy
^tSkobeltsyn Institute of Nuclear Physics, Lomonosov Moscow State University, Moscow 119991, Russia
^uPhysics Department, Università degli Studi Federico II and INFN, Napoli 80126, Italy
^vSt. Petersburg Nuclear Physics Institute, Gatchina 188350, Russia
^wChemistry, Biology and Biotechnology Department, Università degli Studi and INFN, Perugia 06123, Italy
^xDepartment of Physics, Princeton University, Princeton, NJ 08544, USA
^yPhysics Department, Università degli Studi Roma Tre and INFN, Roma 00146, Italy
^zSLAC National Accelerator Laboratory, Menlo Park, CA 94025, USA
^{aa}IPHC, Université de Strasbourg, CNRS/IN2P3, Strasbourg 67037, France
^{ab}Physics Department, Temple University, Philadelphia, PA 19122, USA
^{ac}Physics Department, University of California, Davis, CA 95616, USA
^{ad}Physics and Astronomy Department, University of California, Los Angeles, CA 90095, USA
^{ae}Amherst Center for Fundamental Interactions and Physics Department, University of Massachusetts, Amherst, MA 01003, USA
^{af}Physics Department, Virginia Tech, Blacksburg, VA 24061, USA

Abstract

DISCLAIMER (June 15, 2016): This paper is still work in progress and therefore this version only can give an overview of the status. Comments are appreciated,

yet likely more efficient on a slightly later version of this document. BR

This report describes design, fabrication, commissioning and use of a calibration source insertion system (CALIS) in DarkSide-50 experiment. CALIS deploys radioactive sources into the liquid scintillator veto to characterize the detector response and detection efficiency of the DarkSide-50 Liquid Argon Time Projection Chamber used for dark matter detection, and the surrounding 30 t organic liquid scintillator neutron veto. It was commissioned in September 2014 and used successfully in several campaigns to deploy gamma and neutron sources since then. A description of the hardware and highlights from calibration analysis results are given below.

Keywords:

Dark matter, WIMP, Noble liquid detectors, Low-background detectors, Liquid scintillators, radioactive source calibration

PACS: 95.35.+d, 29.40.Mc, 29.40Gx

1 **Contents**

2	1 Introduction	4
3	2 Design Requirements & Hardware Implementation	4
4	2.1 Purpose	4
5	2.2 Deployment & Articulation Mechanism	6
6	2.3 CALIS enclosure & Scintillator	9
7	2.4 Deployment device	11
8	2.5 Source holder and arms	12
9	2.6 Hardware details and safety features	13
10	2.7 Degrees of freedom of the system	14
11	3 Testing, Cleaning and Commissioning	16
12	4 Calibration Campaigns	17
13	4.1 Radioactive Sources	17
14	4.2 Timeline of the Calibration Campaigns and Stability	18
15	4.3 TPC Calibration	19
16	4.4 Liquid Scintillator Veto	22
17	5 Conclusions	22

18 **1. Introduction**

19 DarkSide-50 is a Liquid Argon Time Projection Chamber (LAr TPC),
20 operated in the Gran Sasso National Laboratory (LNGS) in Italy to search
21 for nuclear recoils induced by weakly interacting massive particles (WIMPs).
22 The first physics result was reported in [1] based on 50 live days of
23 data collected with Atmospheric Argon (AAr), providing the most sensi-
24 tive limit on a dark matter search using a LAr TPC to date with a 90%
25 CL upper limit on the WIMP-nucleon spin-independent cross section of
26 $6.1 \times 10^{-44} \text{ cm}^2$ for a WIMP mass of $100 \text{ GeV}/c^2$.

27 The DarkSide-50 apparatus has been described in detail in [1]. As
28 shown in fig. 1 it features a LAr TPC surrounded by a 30 t liquid scintillator-
29 based veto (LSV) system, placed inside a water Cerenkov veto detector
30 (WCV), both of which measure in-situ and suppress radiogenic and cos-
31 mogenic backgrounds. On top of the WCV is a radon-free clean room
32 (CRH) housing the cryogenic supply system and electronics (Fig. 2). The
33 inside of the LSV is accessible from CRH through four access ports called
34 organ pipes closed by gate valves.

35 *Laser calibration*

36 Electronics gain calibration of the WCV, LSV and TPC is performed
37 with dedicated Laser systems, that are in place in each of the three sub-
38 detectors. The Laser calibration in the WCV is sufficient to veto muons
39 (and their secondaries) with high efficiency. The TPC detector response
40 has been calibrated using the internal ^{39}Ar as well as ^{83m}Kr , that has
41 been added into the LAr recirculation system during dedicated calibra-
42 tion campaigns [1].

43 **2. Design Requirements & Hardware Implementation**

44 **2.1. Purpose**

45 CALibration Insertion System (CALIS) deploys radioactive gamma
46 and neutron sources inside the LSV to study and calibrate the detector
47 response and neutron detection efficiency of the TPC and LSV. This com-
48 plements and extends the physics reach of internal calibration sources
49 and laser calibration.

50 The center of the LSV is about 6 m below the gate valve inside CRH
51 and the 15 cm diameter wide organ pipes are 80 cm off the TPC's vertical

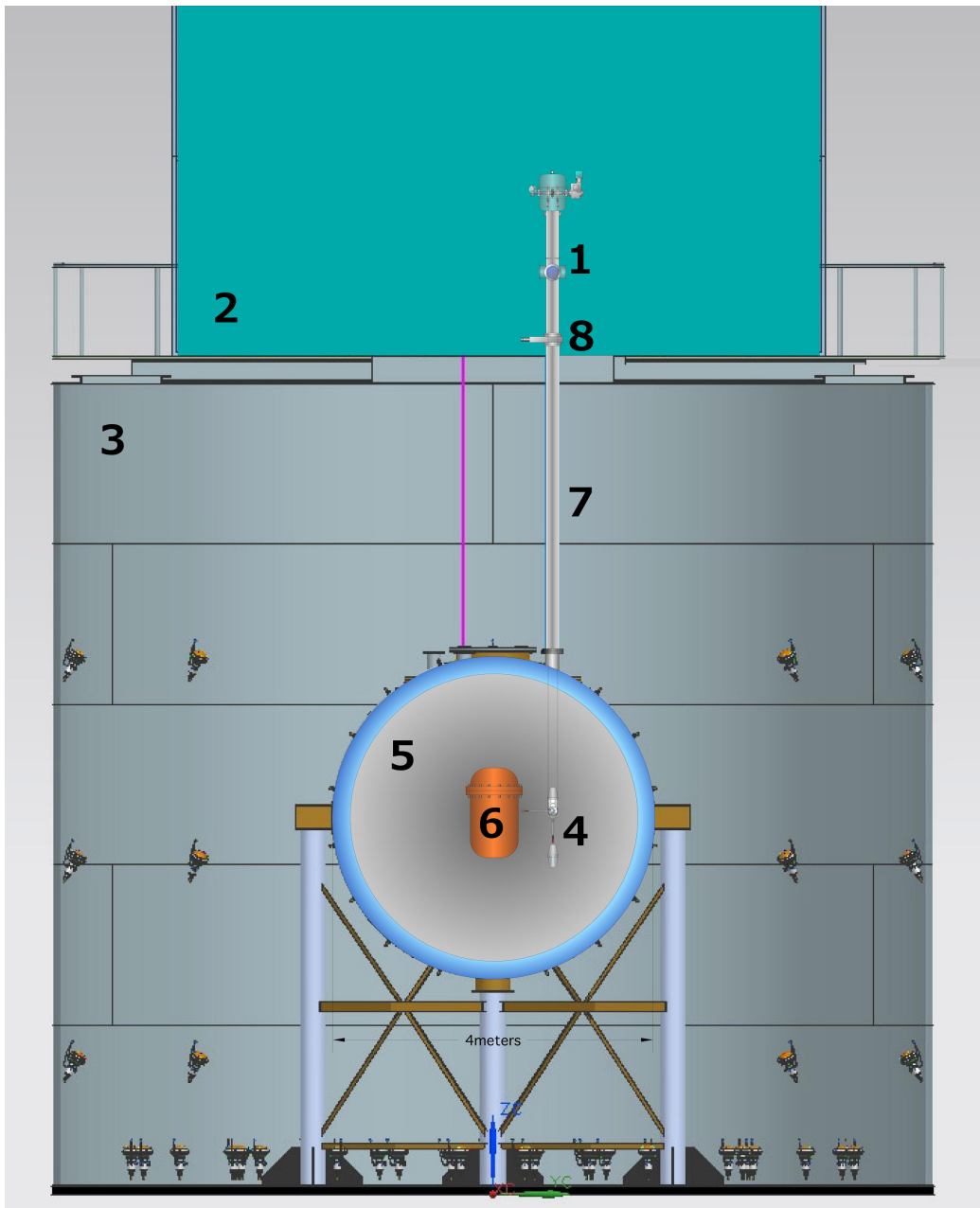


Figure 1: A conceptual drawing of CALIS (1) installed in the radon-free clean room CRH (2) atop the water Cerenkov veto (WCV, 3) and with the deployment device (4) containing the source deployed in the liquid scintillator veto (LSV, 5) next to the liquid argon time projection chamber's (LAr TPC) cryostat (6). The clean room and the LSV are connected through four access ports called organ pipes (only one of which is drawn in the sketch above: (7)). All four organ pipes end in CRH at gate valves (8) which can be manually opened or closed. During normal operations all four organ pipes are closed. Not included in the sketch are tubes connecting the cryogenic systems in CRH to the cryostat in the LSV [2].

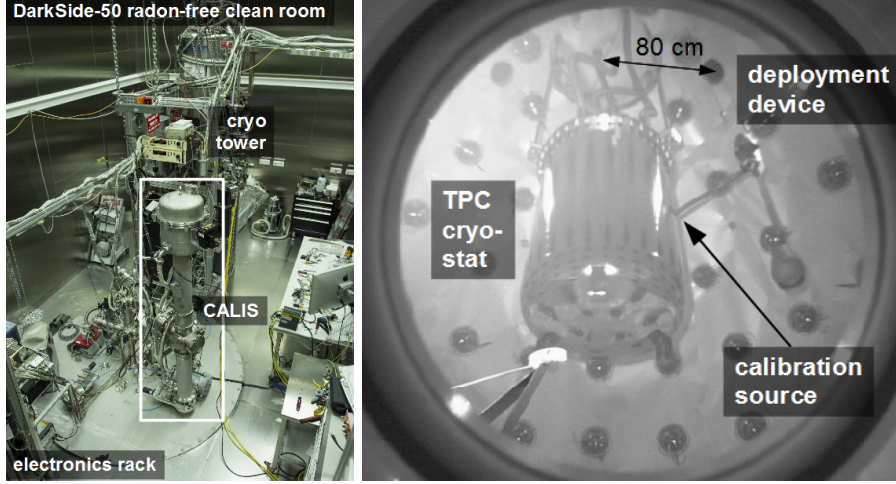


Figure 2: *left*: CALIS after installation inside the radon-free clean room CRH. The organ pipe is 80 cm off-center with respect to the TPC's vertical z-axis. *right*: Photograph taken with a camera looking upwards into the LSV from the bottom. It shows the source deployment device deployed through one of the organ pipes visible on the top right. The arm is articulated and the source is next to the cryostat of the LAr TPC [2].

52 z-axis as shown in Fig. 2. For TPC calibration the radioactive source has to
 53 be positioned in immediate contact with the cryostat, in order to minimize
 54 rate losses through absorption in particular for low energy sources such
 55 as ^{57}Co (122 keV).

56 2.2. Deployment & Articulation Mechanism

57 This requirement precludes a single cable solution deployed from
 58 within a glove box as has been used in several scintillator experiments
 59 [3, 4]. Instead the apparatus consists of the enclosure, which has been
 60 installed in CRH (Fig. 2, left) and the deployment device is attached to
 61 the housing through two stainless steel cables that are wound up on ca-
 62 ble spools and allow the lowering of the device into the LSV, next to the
 63 cryostat (Fig. 2, right).

64 The stepper motor moves both cable spools concurrently and sends
 65 the deployment device into the LSV. An absolute encoder provides its
 66 current position, even in the absence of power. The stepper motor is
 67 controlled via a simple graphical LabVIEW interface, run on a dedicated
 68 laptop, in which the current z-position is shown and a target z-position
 69 can be provided by the operator. Z-positions are given in motor step
 70 counts, an arbitrary unit which has been calibrated outside CRH in meters

in fig.3 the drawing should show the arm articulate towards the left, since when the left spool is engaged, the arm articulates towards the left.

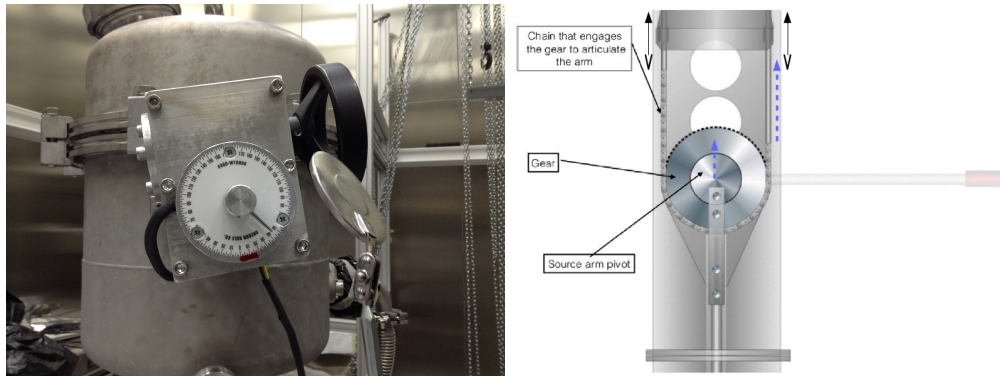
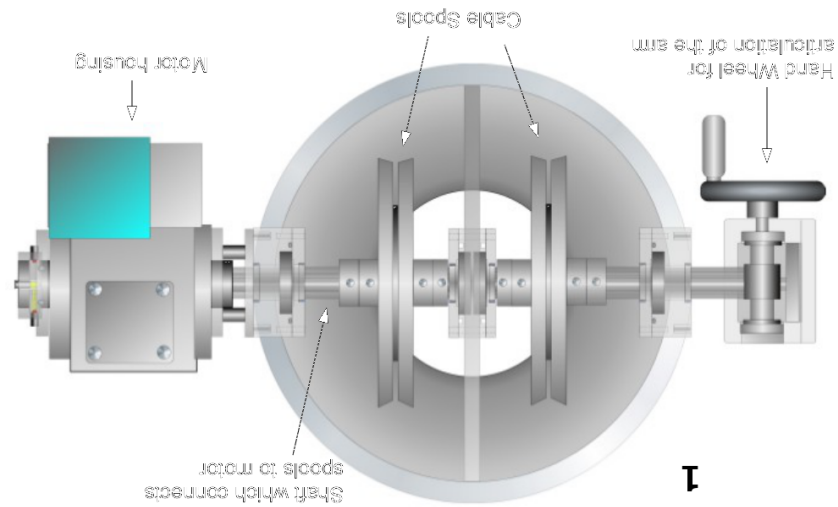


Figure 3: *top*: Inside view of the drive mechanism's components seen from the top of CALIS. The stepper motor inside the motor housing drives both cable spools concurrently, thereby lowering the calibration device into the LSV. An absolute encoder provides the current position of the deployment device. The hand wheel on the left turns the left spool only (*bottom left*). When engaged, it drives the gear to transfer the rotation of the articulation wheel into a rotation of the source arm (*bottom right*). The chain has a guard rail, not shown in the drawing, that ensures that the chain can never come off the gear.

⁷¹ (Fig. 4) and relative to the TPC using the t-drift distribution of calibration
⁷² data (Fig. 13).

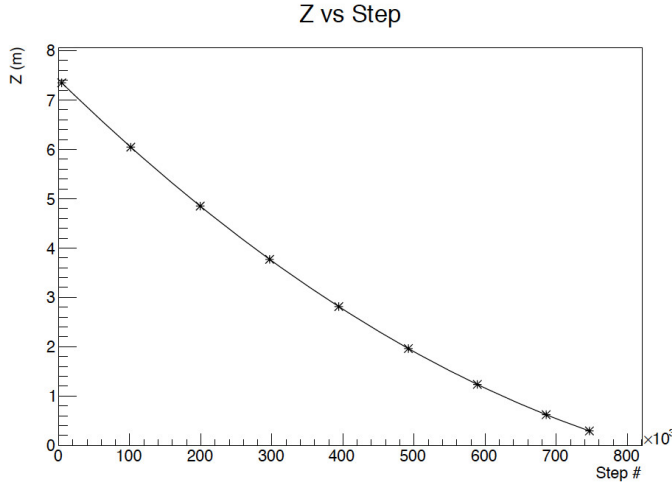


Figure 4: Plot of the z position of the deployment device versus the step position of the motor. The non-linear correspondence between the number of steps and the length of cable deployed arises as follows: As the cable winds around the spool, the winding radius changes, increasing as the deployment device is lifted and decreasing as it is lowered. A motor step count corresponds to a fixed angular distance $d\theta$, yet the amount of cable deployed during this motor step count is $winding\ radius \cdot d\theta$. As the winding radius changes as a function of z position, the fraction of deployed cable per motor step count changes.

⁷³ Articulation of the arm is done manually via the articulation wheel.
⁷⁴ This affects only the cable spool close to the articulation wheel, the left
⁷⁵ one in Fig. 3, thereby shortening the left cable with respect to the right
⁷⁶ cable and engaging the gear through a chain (Fig. 3). As a result the arm
⁷⁷ is articulated and the pivot center is lifted. The non-linearity arising from
⁷⁸ the change in winding radius on the cable spools affects also the amount
⁷⁹ of rotation required by the hand wheel for horizontal articulation of the
⁸⁰ source arm. The degrees on the articulation wheel corresponding to a
⁸¹ horizontal articulation have been calibrated as a function of cable length
⁸² deployed prior to installation in CRH.

⁸³ Articulation and a movement in z-direction are mutually exclusive
⁸⁴ since the articulation of the arm leads to more wound up cable on the
⁸⁵ spool close to the articulation wheel with respect to the other. If then in
⁸⁶ deployment mode both spools would be rotated simultaneously with the

87 same angular speed, the cable close to the articulation wheel would wind
88 up faster than the other, which would lead to a build up of difference
89 in cable length and the deployment device would only be hanging on
90 one cable. In order to avoid an imbalanced z-movement the arm has
91 to be dearticulated fully before a change in z-position can be initiated.
92 This is enforced by an electric switch preventing z-movement, which is
93 disengaged only when the arm is fully dearticulated (vertical).

94 *2.3. CALIS enclosure & Scintillator*

95 Besides providing mechanical support for the deployment device via
96 the cable spools, the CALIS enclosure is an important interface between
97 the radon-free clean room CRH and the LSV, through which sources are
98 exchanged. The enclosure protects the liquid scintillator (LS) and elimi-
99 nates human contact with any traces of harmful liquid scintillator vapor
100 (Fig. 5). It plays the same role as a glove box for similar calibration sys-
101 tems yet with a narrower foot print inside CRH. The liquid scintillator is
102 a mixture of PC and TMB² with the wavelength shifter PPO [2]. It may
103 not get exposed to oxygen or water as is present in normal clean room air.
104 Contamination of LS with ²²²Rn and its long-lived radioactive daughters
105 has to be avoided, too.

106 Going up from the gate valve on which CALIS has been installed,
107 there is a teflon disk that can electrically isolate CALIS from ground,
108 even though during normal operations the CALIS housing is connected
109 to ground. A tripod with a bellow has been used to vertically align the
110 enclosure right after installation on the gate valve. The bellow is con-
111 nected to a 59.4 cm long cylindrical stainless steel enclosure pipe. It has
112 the same diameter as the organ pipe (15 cm) and connects to the view
113 port above by a ring clamp, which plays a critical role in XY rotations
114 (see Sec. 2.7.1). The view port can be opened for handling the source arm
115 and exchanging sources. Everything above the ring clamp forms the up-
116 per assembly. It features a stainless steel cylindrical enclosure that houses
117 the cable drive mechanism, including the cable spools, the stepper motor
118 and the articulation mechanism already described in Sec. 2.2.

²The concentration of TMB has varied during campaigns (see Sec. 4).

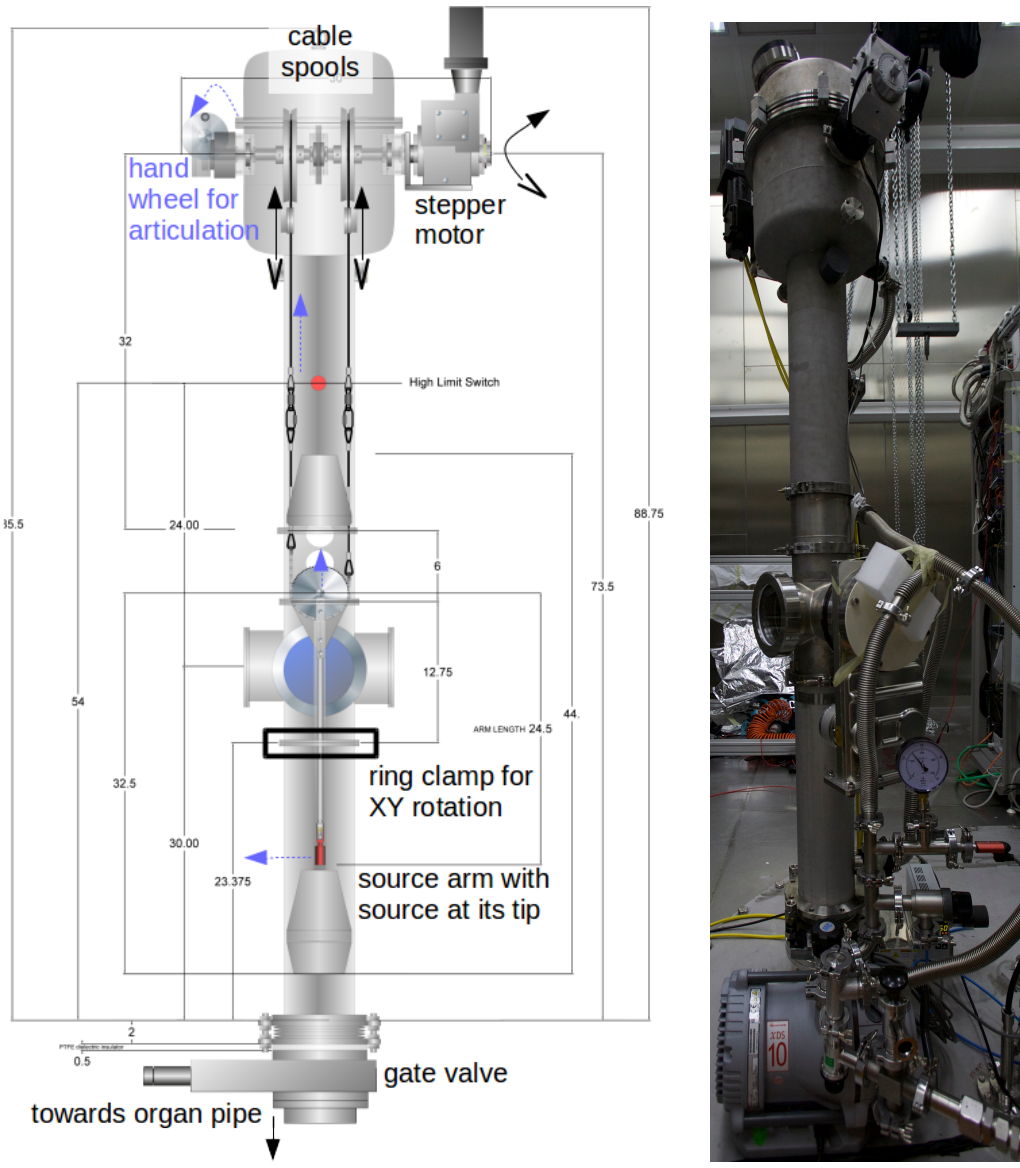


Figure 5: Mechanical drawing of CALIS showing the housing and the deployment device in its home position. Dimensions are in inches. (The total height of 88.75 inches corresponds to 225.4 cm.) The two modes of operation are illustrated: In order to move the deployment device down into the LSV or back up the stepper motor moves both cable spools simultaneously. In order to articulate, the articulation wheel is rotated manually, which affects only the left spool, thereby shortening the left cable with respect to the right cable thereby articulating the arm and lifting the pivot center. The amount of lifting and the amount of rotations until a horizontal articulation is reached has been calibrated prior to installation in CRH (Sec. 3)

119 *Vacuum evacuation (flushing) and nitrogen purging*

120 One of the most important safety features of this system is making
121 sure that the TMB and PC residue on the device are extracted from CALIS
122 prior to opening access ports to exchange source or arms. This is impor-
123 tant for safe working conditions inside CRH as well as for the scintillator
124 and radiopurity.

125 After the insertion of the source arm and closure of the view port the
126 inside of the CALIS housing is filled with normal air, that is damaging
127 to the scintillator. A sequence of evacuations and nitrogen purges re-
128 duces the fraction of air including its contaminants (water vapor, oxygen,
129 radioactivity) to negligible levels. Only after this sequence is finalized
130 the gate valve is opened and the deployment device is introduced into
131 the LSV. Evacuation is achieved with a vacuum pump and exhaust air is
132 removed through dedicated vent lines (Fig. 5).

133 At the end of a calibration campaign, after the deployment device has
134 returned to its home position inside the housing and the gate valve has
135 been closed, scintillator vapor and in particular TMB have to be removed
136 prior to opening the view port. Again a sequence of evacuations and
137 nitrogen purges is employed. By lowering the pressure inside of CALIS
138 below the vapor pressure of TMB and PC, the scintillator evaporates and
139 gets removed through the vent line of the vacuum pump. Once the pres-
140 sure inside the housing stays consistently below the vapor pressure of
141 TMB all scintillator has been removed and the view port can be opened
142 to access the source arm.

143 *Material compatibility*

144 All materials that come in contact with the scintillator veto are made
145 of stainless steel and teflon except for the sealing o-rings which are made
146 of viton. All three materials are certified materials for contact with scin-
147 tillator components TMB and PC.

148 *2.4. Deployment device*

149 The deployment device (Fig. 5) contains the support structure for the
150 arm which holds the source at its end. The device is equipped with ta-
151 pered cones on the top and bottom that ensure that the ends do not get
152 snagged on inner edges of the organ pipe as it is moving up and down.
153 It is attached to the housing by two cables. Swivel hooks are employed in

154 the attachment of the cables to the deployment device that allow the ca-
155 bles to move freely and not get tangled. There are two weights built into
156 the device, one cylindrical in the conical cap above the rotation gear mech-
157 anism and one inside the cones at the bottom end of the device. Both help
158 to minimize any lateral motion or oscillations during deployment and ar-
159 tication and dearticulation especially. It also ensures smooth motion of
160 the deployment device into the organ pipe and back to the home position
161 inside the housing.

162 *2.5. Source holder and arms*

163 A source arm and the source holder are attached to the articulation
164 gear (Fig. 6). Different arm lengths have been prepared with a maximum
165 arm length of 62 cm, the arm length thereby being measured from the
166 pivot point of the rotation gear to the tip of the source holder. This arm
167 length allows the source to be placed in immediate contact with the cryo-
168 stat (Fig. 2, right), as the center axis of the organ pipe is 80 cm from the
169 TPC center and the cryostat has an outer radius of 32 cm. The 62 cm
170 arm was used for deployments in the past calibration campaigns (Sec. 4).
171 Inside the source holder the radioactive source is placed, pressed to the
172 tip and held in place via a spring during deployment, articulation and
173 dearticulation. The source holder is sealed such that no liquid scintillator
174 can enter during the deployment. This has also been verified during each
175 source extraction and no traces of liquid have been found on its inside.



Figure 6: Source holder that connects to an arm and to the articulation gear of the deployment device. The source, here a ^{133}Ba source, is pressed to the tip of the source holder via a spring.

176 2.6. Hardware details and safety features

177 CALIS offers various safety features to ensure that the device runs
178 smoothly, no components are lost inside the detector, avoid any contam-
179 ination of the detector by dirty or incompatible materials, maintain pres-
180 sure and avoid introduction of oxygen or water in contact with the LS
181 and TMB.

182 **Cable strength:** The cables holding the deployment device have been
183 rated for loads over 1300 lbs, while the weight of the deployment de-
184 vice is at the level of 20-30 lbs, thus well below the breaking strength
185 of the cable.

186 **Drive mechanism:** In the event of a power failure, the magnetic break
187 ensures there is no movement of the deployment device. The torque
188 of the servo motor is limited in case of an unexpected load and the
189 risk of breaking the cable is avoided.

190 The speed reducer (gears) is a double worm gear design. The pri-
191 mary worm gear has a 50:1 reduction and the secondary worm has
192 a 82:1 reduction. The input speed of the servo motor is 2400 RPMs
193 and the output is 0.6 RPM and has the weight capacity of 148 lbs. In
194 the event of a power failure the speed reducer has the ability to hold
195 the load at any position without back drive. The speed of the motor
196 has been limited to 0.4 cm/s which minimizes any lateral oscillation
197 of the deployment device during lowering and raising the source.
198 Additionally, this is the maximum speed at which the motor is not
199 overheating.

200 **Manual retraction system:** In the unlikely case of a complete motor fail-
201 ure while the source is deployed, it is possible to manually retract
202 the deployment device back to its home position and close the gate
203 valve. The motor is disengaged, and a wrench is used to manually
204 wind the cable back on the spools and retract the deployment device
205 back above the gate valve.

206 **High limit switch:** A high limit switch is a hardware interlock, that pre-
207 vents the deployment device to hit the cable spools and gears, should
208 it pass beyond the home position in the CALIS housing (Fig. 5).

209 *Neither the manual retraction system had to be used so far nor has the high
210 limit switch been activated during calibration campaigns.*

211 **Light and leak tightness of CALIS:** When the deployment device is next
212 to the cryostat the gate valve is open and data is also taken with the
213 LSV. A prerequisite is that the housing is absolute light tight and
214 pressure leak tight. All view ports are covered with light tight cov-
215 ers when the organ pipe gate valve is open. Both light and leak
216 tightness has been extensively validated throughout the manufac-
217 turing process, commissioning and during calibration campaigns
218 (Sec. 3).

219 **Securing of the source:** All connection points for the source and arm
220 have been secured with two push locking pins that cannot be dis-
221 engaged without a person pressing the pin. In addition, the source
222 holder and the two locking pins are all tethered from outside the
223 view port until they are locked in place eliminating the possibility
224 of accidental falling into the inside of the CALIS housing.

225 2.7. *Degrees of freedom of the system*

226 CALIS has the capability to deploy sources at various positions inside
227 the LSV. Besides the movement along z up to the maximum cable length,
228 there is the possibility to articulate at an angle of θ between 90° and 180° ,
229 where θ is the zenith-angle (Fig. 7). Degrees between 0° and 90° are
230 excluded because the end of the articulation chain is reached at an angle
231 of 90° (see Fig. 3).

232 2.7.1. *Rotation in the XY plane*

233 Below the view port is a sealed connection that has an o-ring seal
234 and uses a ring clamp to compress the seal. The clamp can be slightly
235 loosened to allow the upper assembly (above and including the view port)
236 to be rotated with respect to the lower assembly and the detector. This
237 rotation in the XY plane can even be performed while the deployment
238 device is deployed next to the cryostat, since the seal is helium leak and
239 light tight even when loosened.

240 In principle a rotation in 360° can be done, except when the arm would
241 interfere with the cryostat. This has been used in one of the calibration
242 campaigns to deploy a neutron source directly next to the cryostat and
243 rotated away by 90° in order to study optical shadowing effects from the
244 cryostat (Sec. 4).

My impression is that a drawing to scale with the cryostat, the TPCthe organ pipe and the source arm would be good here

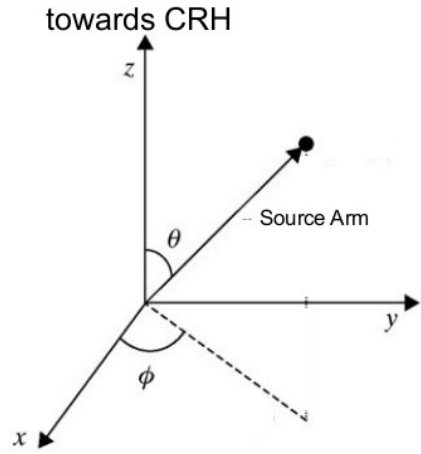


Figure 7: Spherical coordinate system used for establishing the direction of the rotation of CALIS and the articulation of the source arm. θ is kept at 90° when arm is articulated, and at 180° when dearticulated. x -axis is the direction toward the center of the detector.

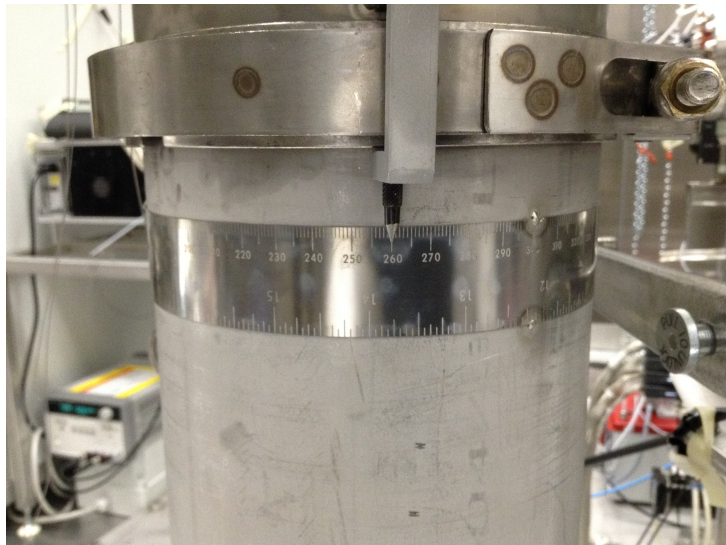


Figure 8: Underneath the view port is the ring clamp with the angle measuring strip underneath. In order to perform azimuthal rotation, the ring clamp is slightly loosened, and the entire upper assembly is rotated with respect to the lower assembly, along with the deployment device. The angle of rotation is read from the strip that goes around the pipe. The strip is in mm, which has then been calibrated in degrees.

245 2.7.2. “No fly” zone

246 Right above the cryostat where there are several supply tubes for the
247 TPC a “no fly” zone has been defined. In this region no part of the
248 deployment device may enter, in particular not the source arm.

249 2.7.3. Default configuration

250 By default the deployment device has been deployed with the longest
251 arm (62 cm), at the center of the active volume of the TPC, with the arm
252 rotated in the XY plane until contact with the cryostat has been made.

253 Other degrees of freedom could involve shorter arm lengths, while
254 longer arm lengths would require hardware modifications to the deploy-
255 ment device. Out of four organ pipes a second one is available for source
256 calibration. (Two organ pipes are not available due to interference with
257 existing infrastructure: the cryogenic tower and electronic rack.) Moving
258 CALIS to a different organ pipe requires a more substantial effort involv-
259 ing a partial disassembly of CALIS and reinstallation on the other organ
260 pipe’s gate valve.

261 **3. Testing, Cleaning and Commissioning**

262 CALIS has been assembled at FNAL from components produced at
263 FNAL and University of Hawaii. After an initial set of basic functional-
264 ity tests at FNAL, CALIS was shipped pre-assembled to LNGS, where it
265 would undergo a comprehensive testing and calibration program. Still
266 outside the clean room CRH, CALIS was installed on a high bay and
267 tested at its full length. Besides testing all details of CALIS (see Sec. 2.6)
268 ranging from testing the functionality of motor controls, high limit and
269 articulation switch to recovery scenarios after e.g. power failures during
270 deployment.

271 An important aspect was the calibration of the sources Z-position as a
272 function of cable length before and after articulation of the source, which
273 is a nonlinear function of motor step counts, as mentioned in Sec. 2.2. Fur-
274 thermore the accuracy and precision of XY- and Z-position of the source
275 was estimated.

276 The results of this testing campaign were reviewed by an internal re-
277 view board and approval for installation inside CRH was granted. CALIS
278 was cleaned according to official cleaning procedures and installed on the
279 gate valve of CRH in September 2014. After installation on the gate valve

280 a focus of testing was the light and helium leak tightness of the system,
281 and the testing of the nitrogen and vacuum systems, as these could only
282 be tested in full after installation. A more detailed description of tests
283 performed at FNAL and LNGS can be found in [5, 6].

284 *XY and Z position*

285 Tests in air and in the LSV's scintillator revealed that the source po-
286 sition accuracy and precision is dominated by uncertainties during artic-
287 ulation. The positioning in z before articulation is highly accurate and
288 precise: The deployment speed is very low, barely visible to the naked
289 eye (4 mm/s), which minimizes the lateral motion during deployment
290 and contact with housing or organ pipe is avoided during deployment.
291 Yet during articulation a swing in XY is arising from tiny laterally imbal-
292 anced forces originating in the pull on the articulating cable.

Tests will be
described in
more detail in
Erin and Bri-
anne's thesis
→ cite them
here.

293 To ensure deployment precision we worked out a procedure to make
294 reliably gentle contact with the cryostat, thereby eliminating the preci-
295 sion uncertainty in XY: After positioning the deployment device in z, the
296 source arm is articulated to horizontal while it is pointing away from the
297 cryostat. Only then the source is brought into contact with the cryostat
298 through a rotation in XY while monitoring the PMT scaler rates, which
299 increase while the source is approaching, yet plateaus as soon as contact
300 with the cryostat is made, even if the rotation in XY continues. This pro-
301 vides a reliable XY and Z-position for the calibration source and has been
302 used throughout calibration campaigns.

303 **4. Calibration Campaigns**

304 *4.1. Radioactive Sources*

305 For the calibration of the LSV detector response and the TPC's re-
306 sponse to electron recoils (ER) we selected ^{57}Co , ^{133}Ba and ^{137}Cs . In a
307 later calibration campaign also ^{22}Na has been deployed. They allow a
308 cross-calibration with ^{83m}Kr , that has been injected in the Ar recirculation
309 system during dedicated campaigns and the internal ^{39}Ar , as they cover
310 the energy range of ^{39}Ar (see also Table 1 and Fig. 9).

311 After a preselection of gamma source energies, detailed studies with
312 the DarkSide Monte Carlo simulation package G4DS [?] were per-
313 formed to select appropriate source activities and check the feasibility
314 and physics reach of various deployment positions. Considering also

possible
upgrade for
fig.16: all
measured
spectra
overlaid
at a fixed
HV: 83mKr,
 $\text{Co}57$, $\text{Ba}133$,
 $\text{Cs}137$ (either
null field or
200 V/cm) -
ask Brianne?
Also for her
thesis?

315 constraints from the LSV and TPC DAQs, sources with suitable activities
 316 were identified for deployment (Table 1).

317 Energy variables are calibrated in photo-electrons (PE) using dedi-
 318 cated Laser calibration runs, in which the single PE charge spectra for
 319 each PMT are fitted and a PE-charge gain is determined. These Laser
 320 runs are also an integral part of a calibration campaign requiring a Laser
 321 run every few hours and at least on each change in DAQ or CALIS con-
 322 figuration, such as drift field changes or source position changes.

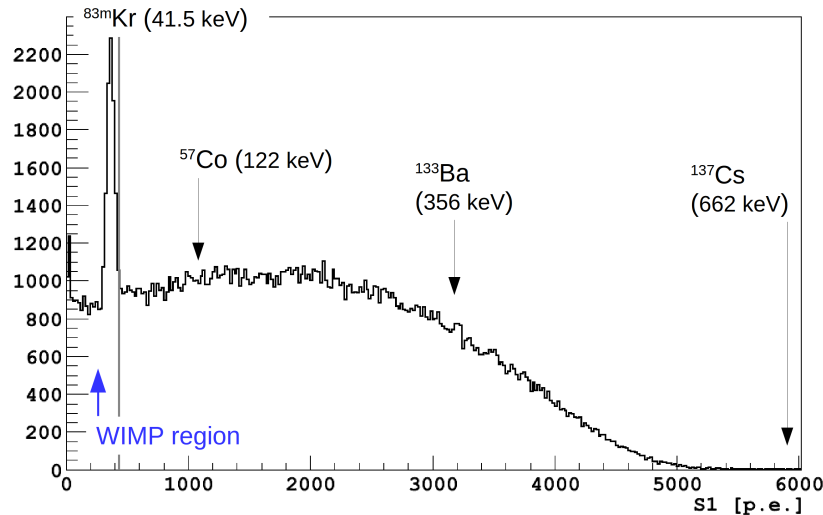


Figure 9: Scintillation spectrum (S_1) at null field showing a ^{83m}Kr peak on the $^{39}\text{Ar} \beta$ spectrum. The energies of the three gamma sources are indicated and cover the full range of the ^{39}Ar spectrum.

323 4.2. Timeline of the Calibration Campaigns and Stability

324 Between October 2014 and April 2016 the following calibration cam-
 325 paigns have been performed:

- 326 • The first extensive campaign involving all gamma sources and both
 327 the high and low activity AmBe neutron source took place in Octo-
 328 ber and November 2014 at LNGS. The TPC was filled with Atmo-
 329 spheric Argon with an inherent trigger rate of approx. 50 Hz from
 330 ^{39}Ar . The liquid scintillator of the LSV contained a PC only scintilla-
 331 tor with $< 0.1\%$ TMB and 1.4 g/l PPO as wavelength shifter.

get the num-
bers for Na22
in the table

has atmo-
spheric argon
been intro-
duced and
underground
argon?

Table 1: Gamma sources deployed in DS-50, ^{39}Ar and $83m\text{Kr}$ [?]. Interaction length is in LAr. Activity of ^{39}Ar has been approx. 50 Hz during AAr filling and negligible in the UAr phase. The Kr source activity varied from campaign to campaign, but was in the range of a few Bq to some tens of Bq.

source	type	energy	half life	interact. length	activity
^{57}Co	γ	122 keV	0.744 y	4.4 cm	35 kBq
^{133}Ba	γ	356 keV	10.54 y	7.5 cm	2 kBq
^{137}Cs	γ	662 keV	30.2 y	9.5 cm	0.65 kBq
^{22}Na	γ	$2 \cdot 511 \text{ keV} + 1274 \text{ keV}$	xxx y	xxx cm	11 kBq
^{39}Ar	β	565 keV endpoint	xxx y	sub-mm	50 Hz
$83m\text{Kr}$	2β	$32.1 \text{ keV} + 9.1 \text{ keV}$	xxx y	sub-mm	

- In January and February 2015 a second campaign focusing on the LSV calibration using the low activity AmBe source was performed. Prior to that the LSV has been reconstituted with 5 % TMB. Two deployments were performed at two different PPO concentrations (0.7 g/l and 1.4 g/l), allowing to study the impact of the PPO concentration on alpha and gamma quenching. (1.4 g/l is our nominal PPO concentration, see also Fig. 14, right)
- In August 2015 a ^{22}Na source has been deployed next to the cryostat for TPC calibration. This was the first gamma source calibration campaign after the UAr deployment within DarkSide-50.
- In December 2015 an $^{241}\text{Am}^{13}\text{C}$ neutron source has been deployed, allowing an in-depth study of the detection efficiency of the prompt neutron recoil signal in the absence of the correlated 4.4 MeV gamma, obfuscating the neutron recoil signal in case of an AmBe source.

As shown in Fig. 10 the calibration campaigns have not affected negatively the light yield or introduced radioactivity into the LSV.

4.3. TPC Calibration

A few calibration results are shown to illustrate the quality of the acquired calibration data and their description in G4DS [?].

4.3.1. ^{57}Co S1 energy

Fig. 11 shows a data-MC comparison of the scintillation signal S1 spectrum of a ^{57}Co calibration source deployed next to the cryostat and close

what does
5 % TMB
mean?
weight %,
volume %?

instead of
the timeline
by Yann
(DocDB)

I
would like
to show the
 Co60 and a
rate stability
plot - in
progress.

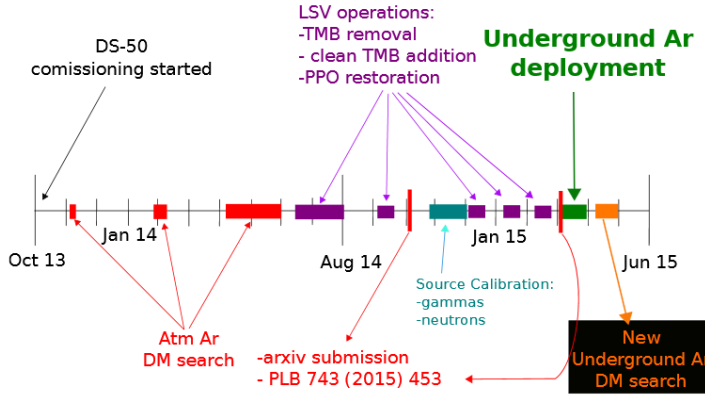


Figure 10: In black the stability of the LSV LY is monitored using internal ^{60}Co emitted from the cryostat steel, in blue the stability of the rate of radioactivity in the LSV is shown. Before and after calibration campaigns both the LY and the rate remain unaffected.

354 to the TPC active volume center. Overlayed is the S1 distribution from an
 355 equivalent selection of G4DS MC simulation.

356 4.3.2. F90 distribution from $^{241}\text{Am}^9\text{Be}$ neutron data

357 Fig. 12 shows good agreement between F90 medians and S1 spectra
 358 measured from $^{241}\text{Am}^9\text{Be}$ neutron data and those derived from SCENE
 359 measurements, which have been used to determine the nuclear recoil en-
 360 ergy scale and NR acceptance regions for the WIMP dark matter search
 361 [? ?].

362 4.3.3. Source position

363 Tests at LNGS established the deployment system's positioning accu-
 364 racy to be about ± 1 cm after a 7 meter journey into the DarkSide-50 LSV.
 365 During the first calibration campaign several runs have been taken with
 366 the source at its central position (731000 motor step counts). Fitting the
 367 t_{drift} distribution at that position for a sequence of runs a systematic shift
 368 vs. time has been observed (Fig. 13, right). The source position has been
 369 on average 157.4 mm below the grid with an RMS of 10.1 mm. Follow-
 370 ing that observed systematic shift with time the deployment procedures
 371 have been revised to avoid such a time dependency in the future and to
 372 improve the deployment precision. It is worth mentioning though that
 373 this does not induce significant uncertainties for calibration data analy-
 374 ses, as the t_{drift} distribution can be measured in-situ on a per-run basis
 375 and hence does not affect our dark matter analysis.

The plot is from Paolo's G4DS talk DS2016, UCLA. Ideally one could get an official copy from the MC paper.

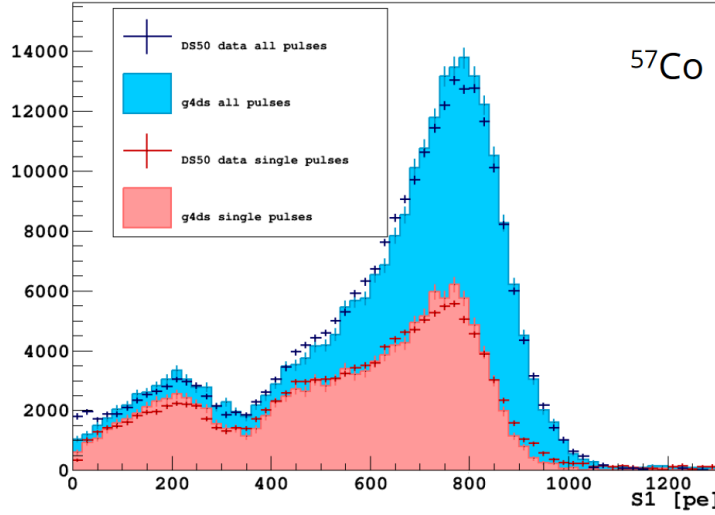


Figure 11: Data-MC comparison for the ^{57}Co source deployed next to the cryostat. In the magenta distribution a single-site interaction requirement has been imposed as for dark matter events and for the blue distribution this constraint has been removed [?].

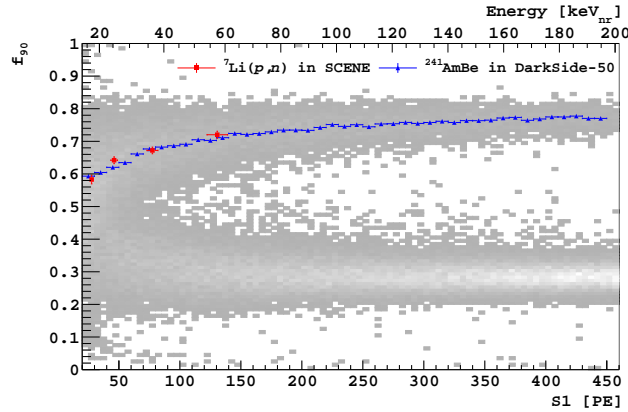


Figure 12: Plot of f_{90} vs. scintillation signal S_1 from a high rate AmBe neutron source calibration of DarkSide-50 in grey, the upper NR band from the AmBe calibration and lower ER band from β - γ backgrounds are visible. Overlayed are f_{90} NR median vs. S_1 from a high-rate *in situ* AmBe calibration (blue) and scaled from SCENE measurements (red points) [?]. There is very good agreement between the two. The high source intensity and correlated neutrons and γ -ray emission by the AmBe source contribute events outside the nuclear recoil and electron recoil bands. (reproduced from [?])

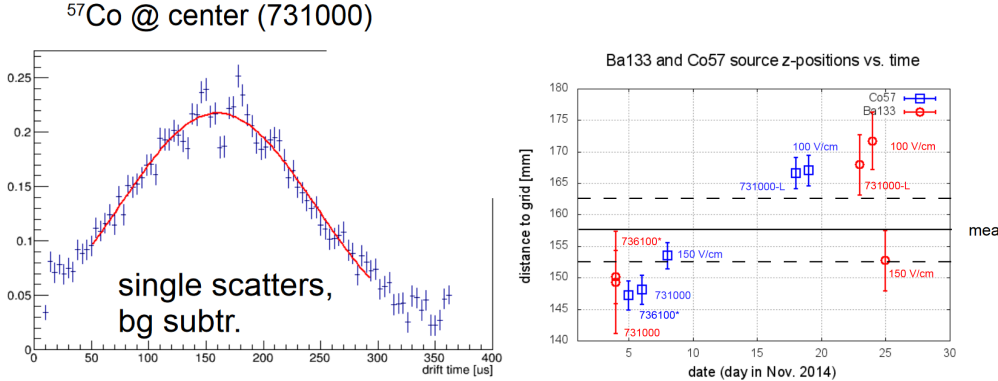


Figure 13: *left*: A t_{drift} distribution encoding the z-position of the ^{57}Co deployed next to the TPC center. *right*: Shift of source position relative to the TPC grid as a function of time when deployed to the same place.

376 For the XY position the distribution of the azimuthal angle in the XY
 377 plane has been studied and a mean of 139 degrees has been observed
 378 with an RMS of 1.2 deg. (One degree corresponds to 6 mm at the outer
 379 cryostat, where the source is positioned.) However an independent XY
 380 reconstruction algorithm gave 142.5 degrees with an RMS of 0.8 deg, so
 381 that systematic uncertainties from the reconstruction dominate over the
 382 XY precision [?].

383 **4.4. Liquid Scintillator Veto**

384 In Fig. 14 (left) a data-MC comparison of the LSV charge spectra from
 385 the ^{137}Cs source deployed in the LSV next to the cryostat is shown [?].
 386 In January and February 2015 the reconstitution of the LSV scintillator
 387 was completed and a second AmBe neutron source calibration of the LSV
 388 calibration was undertaken to further study the various neutron detection
 389 channels in the LSV. With a borated scintillator, a critical aspect of the
 390 neutron detection efficiency is the capability to observe the 6.4 % capture
 391 branch leading to a 1775 keV $\alpha + ^7\text{Li}(\text{g.s.})$ without the accompanying 478
 392 keV γ -ray. As shown in Fig. 14 (right) the de-excitation channel is clearly
 393 observed at around 30 PE.

This is from
DocDB
1288. Ideally
one could cite
a XY paper
here, which is
not published
yet.

394 **5. Conclusions**

395 CALIS is a simple and affordable, yet effective source deployment
 396 system that has been successfully used to deploy sources in the LSV and

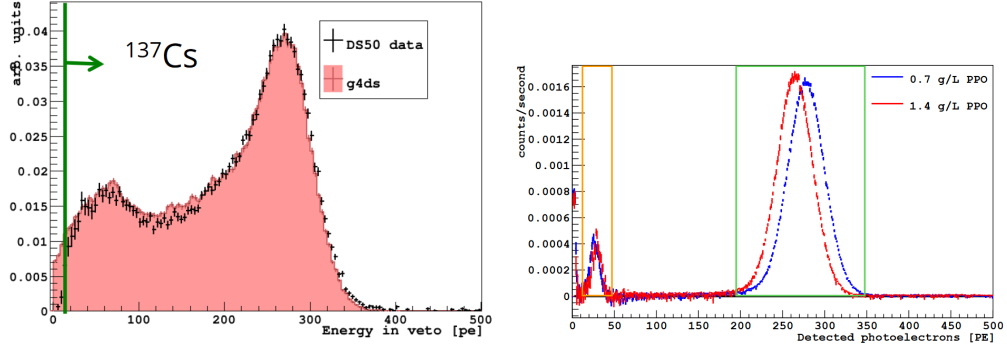


Figure 14: *left:* Data-MC comparison of the LSV charge spectra from the ^{137}Cs source deployed in the LSV next to the cryostat [?]. *right:* Clear detection of the neutron capture signal on ^{10}B in the LSV leading to a 1775 keV $\alpha + ^7\text{Li}(\text{g.s.})$ at ≈ 30 PE (orange box). The peak on the right at ≈ 270 PE (green box) is from the 93.6 % of captures that lead to the ^7Li excited state reaction, with the accompanying 478 keV-ray. The entries below 10 PE are due to PMT after-pulses. Data has been taken before and after varying the concentration of the wavelength shifter PPO in the scintillator with the source rotated 70 cm away from the cryostat. In both cases the deexcitation to ground state is clearly observed.[?]

397 next to the TPC and conduct several successful calibration campaigns. No
398 adverse effects on the LSV or TPC have been noticed.

- 399 [1] P. Agnes, et al., *First results from the DarkSide-50 dark matter experiment*
400 *at Laboratori Nazionali del Gran Sasso*, [Phys. Lett. B, 743, 456 \(2015\)](#).
- 401 [2] P. Agnes and Others, *The veto system of the DarkSide-50 experiment*,
402 [JINST, 11, P03016 \(2016\)](#).
- 403 [3] T. I. Banks and Others, *A compact ultra-clean system for deploying ra-*
404 *dioactive sources inside the KamLAND detector*, [Nucl. Instrum. Meth.](#),
405 [A769, 88 \(2015\)](#).
- 406 [4] H. X. Huang and Others, *Manual Calibration System for Daya Bay Reac-*
407 *tor Neutrino Experiment*, [JINST, 8, P09013 \(2013\)](#).
- 408 [5] B. Hackett, [*thesis title*].
- 409 [6] E. Edkins, [*thesis title*].